Journal of
Ceramic Science
and Technology

J. Ceram. Sci. Tech., **06** [02] 75-86 (2015)
DOI: 10.4416/JCST2015-00001
available online at: http://www.ceramic-science.com

Review

Additive Manufacturing of Bioactive Glasses and Silicate Bioceramics

R. Gmeiner[1], U. Deisinger[2], J. Schönherr[1], B. Lechner[1], R. Detsch[3], A. R. Boccaccini*[3], J. Stampfl[1]

[1]Inst. of Materials Science and Technology, Christian Doppler Laboratory: *Photopolymers in Digital and Restorative Dentistry*, Vienna University of Technology, A-1040 Vienna, Austria
[2]Institute of Glass and Ceramics, University of Erlangen-Nuremberg, D-91058 Erlangen, Germany; Current address: CeramTec GmbH, Medical Technology, D-91207 Lauf, Germany
[3]Institute of Biomaterials, University of Erlangen-Nuremberg, D-91058 Erlangen, Germany
received January 2, 2015; received in revised form March 4, 2015; accepted April 21, 2015

Abstract

This paper reviews the application of a broad range of additive manufacturing technologies (AMTs), including Stereolithographic Ceramic Manufacturing (SLCM/LCM), 3D-Printing, indirect and direct Selective Laser Sintering/Melting (SLS/SLM), Dispense Plotting and Inkjet Plotting on bioactive glasses (BGs) and silicate bioceramics to fabricate a variety of dense and porous structures for biomedical applications (e.g. bone replacement materials). Topical studies in the literature are complemented by recent data of the authors' own work, highlighting the state of the art of additive bioceramic production. The specific characteristics of the technologies used, their advantages and disadvantages and the scope for future research in this field are discussed. To date, many studies focus on 45S5 Bioglass® due to its broad commercial availability. However, other bioactive glass formulations and sol-gel derived BGs are being also considered in the context of AMTs. As the geometrical accuracy and mechanical properties of the fabricated parts strongly vary among the different AMTs, in-depth knowledge of the detailed capabilities of each production process targeted for BGs and other silicate bioceramic materials, as collated in this review, provides information on the basic requirements and challenges for establishing follow-up studies and for possible expansion of the application fields of such additive-manufactured structures.

Keywords: Additive manufacturing, bioactive glasses, silicate bioceramics, scaffolds

I. Introduction

Additive Manufacturing Technologies (AMTs) is the currently used standardized term for those processes (ASTM F2792) where 3D-structures are fabricated by adding material in the form of thin layers, to finally obtain the targeted geometry. In literature, the terms Rapid Prototyping, Layered Manufacturing, Solid Freeform Fabrication, 3D-Fabbing and 3D-printing are frequently used synonymously. In this work, the term AMT will be used, which describes the general manufacturing principle involved in the mentioned techniques.

There are two main categories of techniques to produce ceramic parts by AMT: direct and indirect fabrication techniques. Direct AMTs have the benefit of producing sintered ceramic parts without the need for any further thermal post-processing steps. These techniques melt the ceramic powder particles together by laser interaction and are referred to as selective laser sintering (SLS) [1,2] or electron beam melting (EBM). However, the obtained surfaces are usually rough and local thermal stress problems may arise because of temperature gradients [3] during production. Indirect methods to produce ceramic parts are three-step processes, consisting of three-dimensional printing, thermal debinding, and finally, sintering. Indirect methods involve four basic fabrication techniques, namely (i) laminated object manufacturing (LOM) [4,5], where the feedstock already includes the binder; (ii) extrusion-based techniques, such as robocasting, dispense-plotting and fused deposition modelling (FDM) [6]; (iii) methods relying on stereolithography, e.g. digital light processing (DLP) [7] or laser-based systems (SLA); and (iv) methods based on the fusing of a powder bed, such as 3D-printing and SLS methods, where the binder is present in the feedstock [8].

In general, AMTs are capable of shaping individual geometries on demand, without requiring expensive tooling. This makes AMTs ideal manufacturing processes for applications in medicine and biomedical engineering, where customized, patient-specific geometries are of high benefit. Fields of applications in current clinical use include the fabrication of drill guides for implantology and maxillo-facial surgery [9–12] as well as models [13] for digital dentistry. It is estimated that around 50 000 patients are treated every year using 3D-printed surgical planning instruments [14]. For these applications, the requirements regarding biocompatibility and bio-functional properties of the used materials are mostly achievable with currently avail-

* Corresponding author: aldo.boccaccini@ww.uni-erlangen.de

able AMTs. The present challenge is to provide structures with sufficient structural precision and adequate mechanical properties at a reasonable cost level.

Another attractive approach is the use of AMTs to fabricate cellular, i.e. highly porous, biodegradable scaffolds for tissue engineering [15]. A significant number of research projects have been undertaken towards this direction, with a focus on using material extrusion (e.g. FDM) to fabricate cellular structures made of (degradable) thermoplastic biopolymers like polylactic acid and polycaprolactone [16–18]. An alternative approach is to rely on binder jetting for manufacturing cellular scaffolds made of bioceramics (e.g. calcium phosphate) [19,20].

Conventional ceramic manufacturing techniques have a number of disadvantages, such as cost-intensive production of small-scale series or individual parts like customized designs or prototypes. Additionally, the fabrication of complex parts is very difficult due to the limited capabilities of conventional forming techniques or high tool wear [21] during grinding processes. These limitations again show the need for the development of new production technologies in the ceramic industry. The main limitation in using AMTs for the production of ceramic (and glass) parts is the need to achieve mechanical properties similar to those of conventionally produced ceramics. However, with reasonable build-speeds, reduced costs and the possibility to fabricate 3D-structures with high complexity and resolution, AMTs have moved into the spotlight of the biomedical materials sector. Among the binder-based methods, lithography-based AMTs are likely the most suitable processes for the fabrication of bioceramic or composite objects, since they can process clinically used methacrylate-based light-curing composites [22] without major modifications. In addition, they offer higher precision and better surface quality compared to other AMTs. Using appropriate thermal processing, (stereo)lithography-based ceramic manufacturing techniques (SLCM or LCM) are also capable of shaping fully dense ceramic parts [7,23,24]. The layer-by-layer printing method results in a green part, which consists of ceramic particles and the organic binder. Analogous to conventional ceramic forming, the organic components can be removed during thermal treatment, called debinding. After debinding, the inorganic particles are sintered to obtain the ceramic body, which usually shows a significant amount of shrinkage that has to be calculated and considered in advance.

Using SLCM, dense ceramic structures, comparable to parts built with traditional ceramic manufacturing technologies, could be built (e.g. zirconia (ZrO_2), alumina (AL_2O_3) [7,25] or tricalcium phosphate (TCP) [26]). The potential for bioactive glass powders to be processed with SLCM has been also shown [27]. Indeed, given the increasing interest in bioactive glasses as scaffolds for bone tissue engineering [28,29], there are growing research efforts in adapting AMTs for this type of biomaterials. Bioactive glasses and silicate bioceramics (e.g. glass-ceramics) offer a number of advantages over CaP-based materials for applications in bone regeneration, in particular their high bioactivity, osteoinduction and angiogenic properties [28–32] coupled with the ability to release biologically active ions to induce specific cellular responses and antibacterial effects [33]. Thus the successful manufacturing of bioactive glass and silicate glass-ceramic 3D scaffolds by means of innovative AMTs promises an expansion of the opportunities of applications of such scaffolds, including load-bearing sites. Motivated by the current interest in AMTs for biomedical applications, in the present review we have covered the state of the art of AMTs applied to bioactive glasses and silicate bioceramics. In this context, we discuss the different AMTs investigated, chemical compositions of the silicate systems considered as well as key properties achieved and applications of the materials developed.

II. Lithography-Based Additive Manufacturing of Bioactive Glasses

Among the variety of available AMTs for ceramic part fabrication Stereolithographic Ceramic Manufacturing (SLCM, also called LCM) is arguably the most promising technology regarding material properties and final part strength. This indirect manufacturing process starts with a layer-by-layer build-up of a photoreactive polymer, highly filled with glass, ceramic, or glass-ceramic particles. After green part production, a series of thermal debinding steps is necessary to remove all organic components and to achieve the final sintering density of the ceramic object.

The potential for bioactive glass powders to be processed by SLCM was established in 2012 for the first time [27]. In successive experiments, SLCM was applied to process glass-ceramics and bioactive glass (e.g. Bioglass® 45S5) into dense parts, significantly enhancing their biaxial bending strength [34]. This increase in mechanical strength opens up potential for the use of the BG-based structures in relevant clinical applications such as bone substitutes and scaffolds. Using SLCM it is possible to produce solid bulk glass ceramics as well as delicate scaffold structures with a very homogeneous microstructure, high strut densities and high bending and compression strength (see Fig. 1). Owing to the challenging thermal debinding process, SLCM manufacturing is limited to rather small bulk volumes as gaseous depolymerisation products have to leave the former green body. Nevertheless, parts with a high surface-to-volume ratio can be debinded more easily and can be highly densified during the sintering process. Sintering investigations on test specimens allow for precise shrinkage control, enabling part accuracy in the double-digit micrometre scale.

Indeed stereolithographic printing machines have been developed which are able to process highly viscous slurry formulations into green bodies with an outstanding precision of 25 x 25 μm^2 per pixel as well as 25 µm layer thickness using a digital light processing (DLP) active mask technology [25,35]. Future machine generations will even outperform these accuracy values as laser-writing technologies allow for even tinier stereolithographic writing spots and, at the same time, they will enable larger building areas. Therefore, the technique becomes of great interest for the simultaneous production of small individual ceramic parts in highly complex shapes. The process works well for the 45S5 Bioglass® formulation. In a recent study [34], high biaxial strength, close to natural corti-

cal bone, was achieved for 45S5 Bioglass® test specimens fabricated via the SLCM process. The SLCM-processed glass-ceramic parts have a reduced amount of rather tiny defects, resulting in a high material density, comparable to cast bulk glass materials. The reasons for this improvement can be found in the layer-by-layer building technique of the SLCM process itself as well as in the homogeneous glass powder and slurry quality used [34]. SLCM-processed materials exhibit high density even for the smallest printable structures and filaments, thus the method enables construction of load-bearing scaffolds, potentially opening new fields of implant applications for bioactive glass-ceramics as bone substitute materials.

Fig. 1: Trabecular bone scaffold made of 45S5 Bioglass® and additively manufactured by the SLCM process (10 mm in diameter, 10 mm high); the geometry was generated using µCT images of human femoral bone (pen to scale); Vienna University of Technology.

To work with nature's own trabecular bone topology, microcomputed tomography images (µCT) of an actual human femoral bone are conventionally used to generate the layer information for the SLCM process. Even if it is not possible to artificially construct the complex nanostructure and hierarchy of natural bone, the microstructure of trabecular bone can be reproduced with the precision of a few hundred micrometres, offering some of nature's structural benefits due to its hierarchical porous and lightweight design. In a next step, 45S5 Bioglass® scaffolds were produced using slurry formulations evaluated in previous studies [27, 34]. To avoid too much distortion of the part owing to viscous flow of the glass during sintering and to reduce internal thermal stresses between sections of different volumes, the final sintering temperature was reduced to 950 °C. Sporadic filament cracking occurred in some scaffolds mostly at intersections between delicate scaffold strands and more bulky sections. Nevertheless optical inspections showed impressive overall part quality down to the microscopic level.

To demonstrate further SLCM possibilities it is possible to enhance the structural strength of the bioactive glass scaffolds for specific load-bearing scenarios by adding artificial support structures into the natural trabecular design. These modifications reduce the overall scaffold porosity but could help in specific implant scenarios (e.g. femoral implants) (see CAD data: Fig. 2). In this scaffold design, sections with natural hierarchical pore structure should be able to promote vascularisation ingrowth whereas artificial structural backbones will support the implant during the resorption and bone formation process. A few examples of such auxiliary structures are shown in Fig. 2 (CAD data) and Fig. 3 (manufactured parts). Simple beams can act as vertical support against compression forces, whereas more complex structures (e.g. honeycombs) can support the structure against shear forces or multiple load-bearing scenarios. At the Vienna University of Technology, the author's team in collaboration with the Erlangen Institute of Biomaterials, is currently investigating potential benefits of such enhanced scaffold designs regarding their mechanical compression stability. With this technology, it could become possible for bioactive glass structures to meet specific, patient-related implant requirements not only in terms of shape but also regarding their mechanical properties for load-bearing applications.

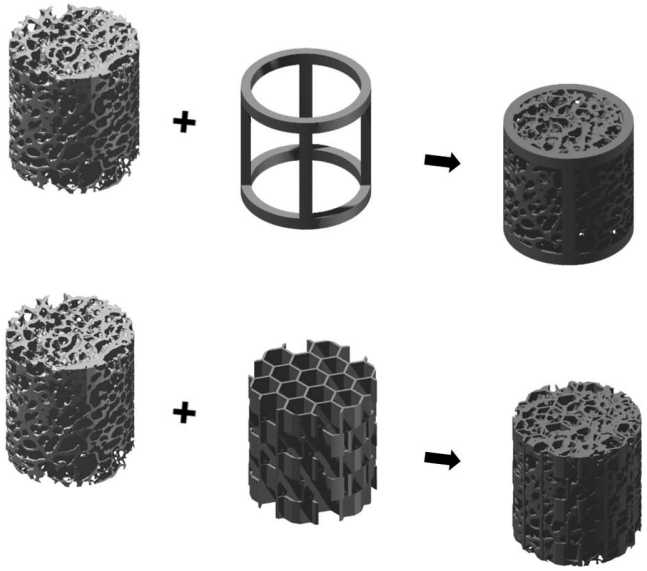

Fig. 2: Trabecular bone scaffold with different artificial support structures; simple barrel rings and beams to enhance vertical compression strength (top); shifted honeycomb structure to enhance structural strength for combined load scenarios (below); CAD files processed with Autodesk Inventor®.

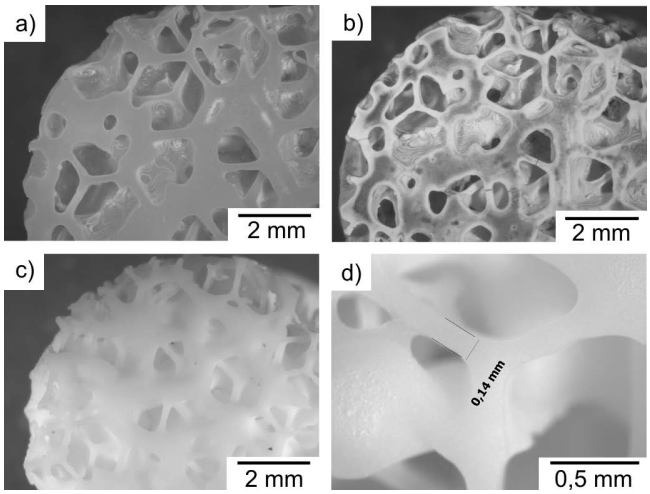

Fig. 3: Trabecular bone scaffold with artificial support structure (shifted honeycomb structure); microscopic images of: green body after stereolithographic printing (a), after thermal debinding (b), final sintered part (c), enlarged detail of final scaffold strands (d); made by SLCM process, Vienna University of Technology.

Due to its broad commercial availability, 45S5 Bioglass® has acted as a precursor material for SLCM process evaluation and development, paving the way for the use of other bioactive glasses and glass-ceramics for medical implant applications and for tissue engineering scaffolds. Indeed an increasing number of current studies involve alternative glass formulations to the standard 45S5 Bioglass® composition in order to enhance the biological activity of the material by specific ion releasing capability and to control the degradation rate of the silicate material [33, 36]. It is well known that a high degradation rate of the silicon-rich interface layer rapidly changes the pH-value around the implant, sometimes leading to necrosis problems of ingrowing and surrounding tissues. Alternative bioactive glass compositions, such as the 13–93 formulation [37], show slower resorption rates, which should lead to superior tissue ingrowth and lower inflammatory risk. Other compositions of relevance are boron-containing silicate compositions or also borate glasses, given the positive effect of boron on osteogenesis and angiogenesis [38, 39]. Future research should therefore focus on the adaptation of the SLCM technique to a variety of novel bioactive glass chemistries.

It is interesting to add that soft lithography, a technique useful for replicating structures applying elastomeric "soft" stamps, mostly polydimethylsiloxane, has been used to surface structure 45S5 Bioglass® substrates [40]. With the use of micromoulding, a BG slurry was forced to flow through channels created in an elastomer stamp. After drying, layers deposited on an amorphous carbon substrate were sintered. Free-standing glass-ceramic structures with high aspect ratio were obtained with lateral resolution better than 1 µm, which were used to investigate the behaviour of osteoblast-like MG-63 cells and rat mesenchymal stem cells (rMSC) on micro-patterned bioactive glass surfaces [40].

III. 3D-Printing of Bioactive Glasses

3D-printing is one of the AMTs based on a powder bed. The principle of 3D-printing is illustrated in Fig. 4. Layer by layer, a liquid binder is printed onto a powder bed, gluing the powder together in the desired areas. After each printed layer, a new layer of powder is deposited onto the building platform via a counter-rotating roller or a doctor blade. These steps are repeated until the designed part is fully printed. During the 3D-printing process the unglued powder serves as support, so that complex parts with undercuts or cavities can be realized. However, in the design of the parts the removal of unglued powder has to be taken into account.

A high free-flowing capability of the powder is required to ensure a homogeneous recoating and a high quality of the powder bed. In this regard, both particle morphology and size have a significant influence, with spherical particles exhibiting a much better free-flowing capability than anisotropic or platelet-like particles. Larger powder particles possess a better free flowing capability than smaller particles; however, the printing resolution is much better for smaller particles. Often spray-dried granules are used for 3D-printing, providing an excellent free-flowing behavior and ensuring adequate printing resolution. A particle or granule size of 20 – 40 µm is regarded as optimum, as with this particle size a layer thickness of approx. 100 µm can be achieved (as a rule of thumb ~ 2 – 3 times the middle particle diameter), and thus, a satisfactory resolution of the printed part is possible. Larger particles (> 100 µm) usually lead to increased porosity of the printed structure, owing to the larger voids between the particles. On the other hand, powders smaller than 20 µm cause capillary forces that lead to strong migration of binder into the powder bed and thus to a reduced printing quality.

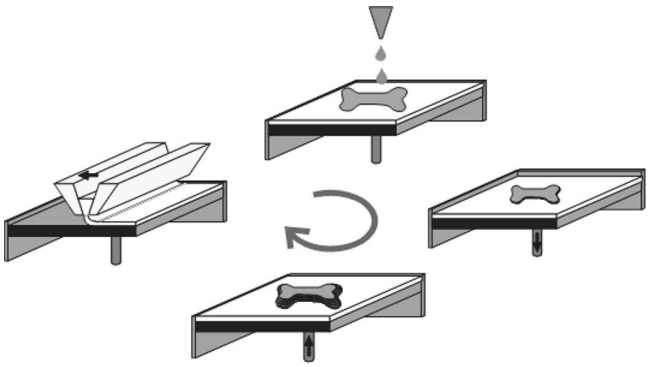

Fig. 4: Principle of 3D-printing: the process steps, namely recoating the powder bed and printing of liquid binder to glue the powder in specific areas are repeated layer by layer until the 3D part has been built.

Typically, water-based systems are used as binder materials. The binder glues the powder particles together, forming a stable three-dimensional part. Thus, the wettability of the binder has to be adapted to the specific powder. Whereas ceramic powders more easily absorb moisture, the wetting of glass powders is more difficult due to their hydrophobic nature [41]. However, to improve the gluing capability, in most cases an additional binder component, e.g. dextrin, is additionally mixed into the powder, ensuring a more homogeneous distribution of binder in the printed part.

Ceramic and glass 3D-printed structures usually have to be heat-treated after the moulding process. First, a binder burn-out step is applied to ensure complete burn-out of all organic additives (also called debinding). Due to the porous nature of 3D-printed parts, the effusion of the developed gasses is usually achieved. 3D-printed glass-containing samples can be sintered to almost full density (0.36 % residual porosity) [41]. This enhanced densification can be related to the sintering mechanism of glass, viscous flow, which leads to a stronger mass flow and enables the efficient closing of pores. However, crystallization effects have to be taken into account when optimising the heat treatment parameters for sintering glass samples. This is especially important for 45S5 Bioglass® due to its readiness to crystallise [42]. During sintering of 3D-printed glass samples, anisotropic shrinkage (40 % in z-direction, 30 % along slow axis and 16 % along fast axis) may occur, which can be related to the layer-by-layer manufacturing method [41]. However, isotropic shrinkage characteristics have also been reported [43].

Regarding the fabrication of silicate-based scaffolds, 3D-printing has mainly been used for the development of

glass/ceramic composite scaffolds, whilst the fabrication of amorphous glass structures has been less investigated.

Hydroxyapatite (HA)/apatite-wollastonite (A/W) glass-ceramic composites were fabricated from A/W-glass powder and HA powder, which were previously mixed in a suspension with maltodextrin as additional binder component. After drying and grinding, a homogeneous size distribution with a mean diameter ~70 µm [44] was achieved. Although the particle size was relatively large, a layer thickness of 100 µm could be obtained. The particles were glued using a water-based binder. During sintering, the porosity of the 3D-printed samples could be reduced in dependence of the sintering temperature, from > 51 % to 2.5 %. After sintering of the HA-A/W-composite, besides hydroxyapatite also the calcium phosphate silicate phases and tricalcium phosphate phases were present. 3D-printed and sintered samples revealed a Young's modulus in the range 7 – 30 GPa and a 3-point bending strength of 50 – 150 MPa, sufficient for applications as bone implants. *In vitro* bioactivity and biocompatibility tests were performed: after soaking sintered samples in SBF for only one day, an apatite layer started to form on the surface, showing a high bioactivity of the final material. Human osteoblast cells, seeded for six days on the 3D-printed and sintered scaffolds, proved the non-toxicity of the samples, cell adhered well on the surface and showed normal morphology.

A mixture of calcium phosphate ceramic and 45S5 Bioglass® was 3D-printed employing a cementing reaction during the printing process [45]. This was realized by printing an aqueous-based binder containing orthophosphoric acid and pyrophosphoric acid into a powder bed of spray-dried granules of 40 wt% β-TCP and 60 wt% 45S5 Bioglass®. During the resulting cementing reaction, dicalcium hydrogen phosphate (DCPD) and dicalcium pyrophosphate (DCPP) were formed. The spray-dried granules had a mean granule size of 41 µm, allowing a layer thickness of 50 – 75 µm. To improve the strength of the 3D-printed samples, they were sintered at 1000 °C, resulting in a final phase composition containing rhenanite ($NaCaPO_4$) and wollastonite ($CaSiO_3$). The bending strength of sintered samples was measured to be 14.9 ± 3.6 MPa. In comparison to pure ceramic 3D-printed scaffolds, the increase of strength due to sintering of the ceramic/glass mixture was higher, possibly due to the viscous-phase-assisted densification during sintering. As an example, a patient-specific implant, derived from CT data, was printed without the incorporation of additional macropores.

Another composite incorporating calcium phosphate, which has been 3D-printed, is HA/13-93 bioactive glass [43]. For the fabrication of the printing powder the glass frit (d_{50} = 3, 8 and 14 µm) and 0 – 60 wt% calcined HA powder (d_{50} = 3.6 µm) were mixed in an aqueous-based slurry with 6 wt% dextrin binder and polyacrylic acid as lubricator, the mixture was then dried and ground in a swing mill. Additionally, 10 wt% dextrin was added to the mixture as binding agent inside the powder bed. A water/glycerol solution (7:1) was used as printing binder, the layer thickness was 150 µm. As the density of the 3D-printed parts was only 40 ± 5 %, a subsequent sintering step was applied. By means of sintering at temperatures up to 810 °C, almost dense samples (~ 97 % theoretical density, T. D.) without crystallisation of the 13 – 93 glass were achieved. For pure glass samples, sintering was driven by viscous flow. However, with increasing HA content, the percolation of HA particles was seen to increasingly influence the sintering process, requiring higher sintering temperatures, and finally, leading to highly porous samples for an HA content of 60 wt%. 3D-printed and sintered samples with up to 20 wt% HA exhibited a bending strength of ~ 70 MPa and a Young's modulus of ~ 80 GPa. For 40 wt% HA, cubic samples of 20 x 20 x 20 mm^3 with round macropore channels of 2.0, 1.5 and 1.0 mm diameter were fabricated by means of 3D printing (Fig. 5) [43]. The diameter of the channels could be reproduced with an accuracy of 15 ± 5 %.

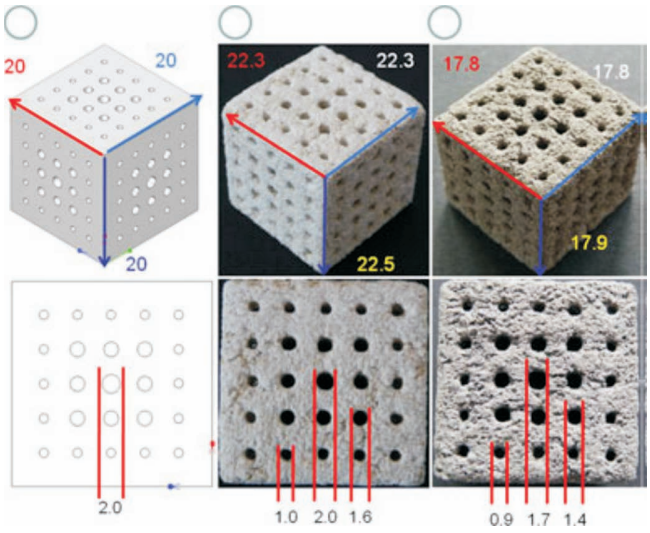

Fig. 5: Computer model (a), and photograph of 3D-printed green body (b) and sintered (at 720 °C at 2 K/min) glass/HA composite structure (c). Labels indicate dimensions in mm, according to ref. [43] (Reproduced with permission of Wiley).

Another possibility to achieve glass/ceramic composites is the *in situ* formation of a silicate glass-ceramic [46]. In a previous approach, a lithium aluminosilicate (LAS) glass frit was used as a precursor glass powder and was milled into two different particle size distributions (d_{50} = 75 and 223 µm). A water-based binder was printed onto the powder bed and cross-linked at 125 °C for 24 h. During sintering up to 860 °C for 8 h the crystalline phases developed. The final glass-ceramic contained β-spodumene solid solution together with a secondary phase of lithium disilicate Li_2SiO_3. For 3D printing, the layer thickness was varied between 80 and 200 µm. However, best printing qualities were achieved with a layer thickness of 100 µm and using the finer powder. With optimised printing parameters and powder distribution, cubic samples of 1 x 1 x 1 cm^3 with pore channels of 2 x 2 mm^2 in size (square cross-section) and strut diameters of 1 x 1 mm^2 could be successfully 3D-printed. However, although a glass phase was present during sintering, the crystallization likely started prior to full densification, resulting in a strut porosity of 34 – 41 % T.D. Nevertheless, for samples with a total

porosity of 64 %, strength of 15 ± 3 MPa was measured in compression tests.

Besides glass/ceramic composites, also pure bioactive glass samples (13 – 93 composition) have been fabricated via 3D printing [47]. The glass frit was milled to a mean particle size of ~ 46 µm, suspended with 6 wt% dextrin in water, dried and ground. The selected areas per layer (layer thickness of 150 µm) were glued with a water/glycerol (7:1) solution. A porosity gradient parallel to the printing direction was found, which can be explained by an inhomogeneous migration of the liquid binder into the porous powder bed. Sintering of the 3D-printed parts was performed at temperatures between 742 °C and 795 °C, leading to full densification of the samples. Higher sintering temperatures were avoided because of crystallisation effects. Different sample geometries were realised, such as cylinders, rectangles and samples with more complex shape.

Altogether, it can be stated that 3D-printing of glass and glass-containing ceramic powders is a very promising AMT, enabling the fabrication of relatively strong glass and glass/ceramic 3D scaffolds. The macropores as well as micropores inside the struts can be tailored with CAD data and by varying the sintering parameters. In this way it is possible to obtain dense struts, thanks to viscous flow sintering of the glassy phases, as well as highly porous struts, e.g. by exploiting crystallisation effects. The results in the literature also reveal that the surface quality of the printed scaffolds is limited by the size and morphology of the applied powder.

IV. Selective Laser Sintering (SLS)/Selective Laser Melting (SLM)

Another AMT based on selective densification of a powder bed is Selective Laser Sintering (SLS), sometimes also called Selective Laser Melting (SLM). Analogous to 3D-printing, a powder bed, consisting of a free-flowing powder, is fused (in the case of SLS by a laser) in previously defined areas. After each densification step the powder is recoated with a certain layer thickness (Fig. 6).

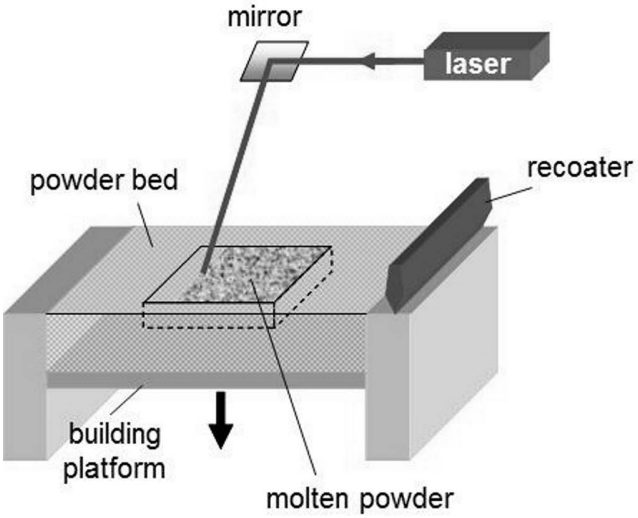

Fig. 6: Schematic process of Selective Laser Sintering (SLS): The powder bed is scanned by a laser, which melts the powder particles, thus fusing them to finally form a 3D part.

In contrast to 3D-printing, the powder bed can be readily sintered using a laser, melting the powder in the powder bed and densifying it. Thus, no subsequent debinding or sintering step is necessary. However, it is also possible to fabricate green bodies via SLS, e.g. by mixing a thermoplastic polymer into the powder bed, which is melted by the laser and fuses the glass and/or ceramic particles together. In this process mode, after the AM step the binder is burned out and the part is conventionally sintered.

In both cases, it is important that the laser interacts properly with the material; meaning that the material has to readily absorb the laser energy. In this case, also the wavelength of the laser is significant. For SLS of ceramics and glasses, typically a CO_2-laser is applied. Other relevant parameters of SLS, which have to be adjusted to every new material, are the laser energy itself as well as its scan speed and scan spacing (i.e. the overlap of neighbouring lines during the scan).

Direct SLS

Glass-based powder systems are particularly suited for the SLS process as the contained glass can be melted by the laser energy, binding at the same time other possible components, for example ceramic particles. The melting and cooling processes are very fast, clearly reducing the production time of the scaffolds compared to the conventional moulding process including a sintering step. Although the glasses are melted in a very short time and no dwell times are kept, crystallization of glasses during the SLS process has been observed. SLS has been used to produce pure bioactive glass scaffolds as well as glass/ceramic composites.

For example, pure 45S5 Bioglass®-based scaffolds have been fabricated via SLS [48]. For this, a glass frit with a particle size < 100 µm was used. Although the particles were irregular-shaped and had sharp edges, the free-flowing capability was sufficient (possibly due to their relatively large size). For SLS, a micro laser beam with a power of 6.0 – 30.0 W was scanned across layers of 0.2 mm thickness. 3D scaffolds (27 x 27 x 5 mm^3) with unidirectional pore channels of 2 x 2 mm^2 and a length of 5 mm in z-direction were fabricated (struts: 2.5 x 2.5 mm^2). At a low laser power, necking between particles was observed, while at a high laser power, holes and sinking of the powder layer were observed. These effects could be related to melting processes owing to the low viscosity of the glass, enabling a viscous flow into the powder bed. As optimal laser power 15.0 W was determined, resulting in dense samples with a high degree of crystallization and the highest fracture toughness (0.65 $MPam^{1/2}$) in the test series. Although the heating and cooling processes during SLS are very fast, the process leads to crystallization of the 45S5 Bioglass® with $Na_2Ca_2Si_3O_9$ as the major crystalline phase, similar to conventionally sintered Bioglass® scaffolds [49].

In another investigation, bioactive glass of composition 58S was used as the basis for SLS of 58S/graphene composite scaffolds [50]. Nanoscaled sol-gel-derived 58S glass powder was dispersed with different amounts of graphene (0 – 1.5 wt%), dried and ground, using a pestle. SLS was performed under nitrogen atmosphere to prevent oxidation of the graphene. The laser power was set at 7.5 W,

the scan speed was 100 mm/s and the laser spot size was 1 mm. Scaffolds with an interconnecting porosity and pore channels of approx. 0.8 mm in all three directions could be successfully fabricated via SLS. Independently of the graphene addition, partial crystallization of the 58S glass to wollastonite ($CaSiO_3$) was observed. The addition of 0.5 wt% graphene to 58S BG achieved the highest compressive strength (~ 49 MPa) and fracture toughness (1.9 $MPam^{1/2}$) of these 3D scaffolds. Bioactivity was investigated using simulated body fluid, where after seven days of immersion a HCA layer formed. *In vitro* tests with MG-63 cells suggested a good cell biocompatibility of the SLS composite scaffold [50].

Wood *et al.* compared the SLS fabrication of an *in-situ*-formed apatite-mullite glass-ceramic to a mixture of crystalline hydroxyapatite and phosphate glass [51]. For the *in-situ*-formed glass-ceramic, a glass of the composition $4.5SiO_2 3Al_2O_3 1.6P_2O_5 3CaO_2 CaF_2$ was melted, quenched and milled. Final particle sizes were sieved to sizes in the ranges 0 – 45 µm, 45 – 90 µm, 90 – 125 µm and > 125 µm. The HA/phosphate glass mixture was prepared from commercially available HA powder (~ 100 µm) and 2.5 – 20 wt% phosphate glass of the system $P_2O_5 CaO Na_2O$, which was milled to a particle size < 20 µm. The laser spot diameter during the SLS experiments was kept at 1.1 mm and the layer thickness was defined to be 0.25 mm.

For the *in-situ*-formed glass-ceramic, crystallisation of fluoroapatite with very small amounts of mullite and aluminium phosphate occurred during the SLS process. Mono- and multilayers could only be produced for particle size in the range 0 – 45 µm and a 1:1 mixture of 0 – 45 µm and 45 – 90 µm within a very small process window with low laser energy (2 – 3 W) and with relatively low scan speed (1 mm/s). However, the laser-sintered layers were very fragile. In contrast, the HA/phosphate glass mixture could be laser-sintered within a broader range of parameters. Multi-layered structures without additional incorporation of macropores were laser-sintered with 10 vol% glass and a scanning speed of 10 mm/s. However, owing to insufficient wetting of the glass phase on HA particles, the resulting structure was very weak and insufficient interlayer bonding was observed. For the HA/phosphate glass composite also the SLS fabrication of 3D-structures with unidirectional pores was shown [52]. A glass frit of composition 50 mol% P_2O_5, 35 mol% CaO and 15 mol% Na_2O was milled to a mean particle size < 20 µm and mixed with spray-dried, sintered HA granules of 20-50 µm in diameter. SLS of glass monolayers was performed with a CO_2-laser. The laser power was varied from 4 to 10 W, the scan speed between 50 and 300 mm/s. Reproducible results were achieved for a power of 4 W and a scan speed of 100 mm/s. However, to fabricate composite multilayers with a layer thickness of 100 µm, the scan speed had to be reduced to 40 mm/s, as otherwise warping of the first layers occurred. It was shown that multilayer HA/phosphate glass structures with rectangular pore channels of 1 x 1 mm^2 in cross-section could be fabricated without delamination.

As mentioned above, during direct selective laser sintering the glass is melted and forms a liquid phase. Owing to the porosity of the powder bed and the surface tension of the liquid glass, the glass phase can migrate towards the middle of the scanned line, leaving spaces to both sides. When the laser scans the next line in this layer, only very few connections between the neighbouring glass lines are formed, although the lines scanned by the laser usually overlap sufficiently (up to ¾). Thus, very porous and fragile constructs with a typical net-like structure, also described as "surface bands" (Fig. 7), are built. These porous structures can be further densified by means of impregnation or post-processing heat treatment [51 – 53].

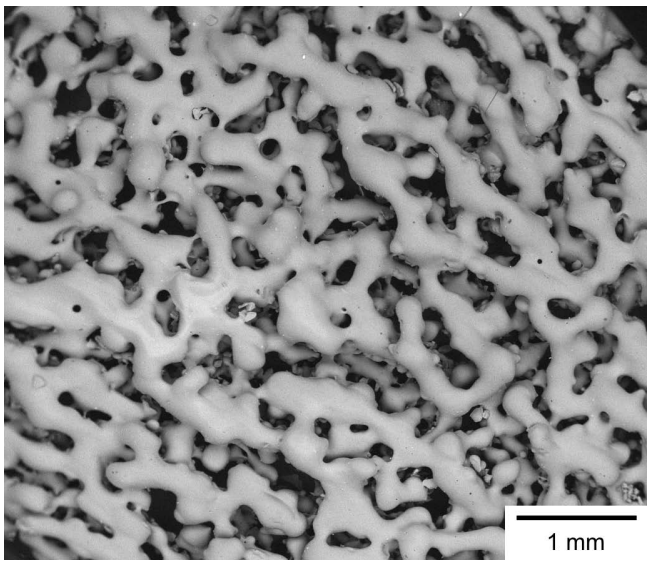

Fig. 7: Typical network-like structure (surface bands) of selective-laser-sintered glass (here: phosphate glass of the system P_2O_5-CaO-Na_2O, unpublished data of author UD).

The appearance of surface bands and "balling" effects can be reduced when the powder bed is heated to a temperature slightly below the melting point. This is difficult for the direct SLS of glasses, as comparatively high temperatures would be needed, complicating the whole machinery of a SLS device. However, using the indirect SLS process, where a green body is fabricated by SLS and subsequently sintered, heating of the powder bed to the required temperatures (below the melting point of binder) is relatively easy to realize. Besides the difficulties in producing dense layers by direct SLS, crystallization of the bioactive glass can occur during the SLS process. For these reasons, the indirect SLS process seems to be more promising for exact and reproducible fabrication of glass parts with high resolution [52].

Indirect SLS

The indirect SLS process has also been used to fabricate pure glass scaffolds and glass-ceramic samples. For the fabrication of 13 – 93 glass scaffolds [54], the 13 – 93 glass frit was mixed with 40 – 50 vol% stearic acid as binder and dry-milled. For SLS a CO_2-laser with a laser beam diameter of 0.46 mm was used. The scan spacing was set to 0.23 mm, which corresponds to an overlap of 50 %. The layer thickness was 76.2 µm and the part bed was heated to 60 °C, which is just under the melting point of the stearic

acid binder (69 °C). Thus, only low energy of the laser was needed to melt the binder, which fused the glass particles together to form a relatively strong body. It was shown that a minimum of 15 wt% binder was needed for laser-sintering scaffolds with sufficient strength for handling and removal of non-sintered powder (e.g. from the macropores). On the other hand, higher binder content increased the shrinkage during subsequent sintering and reduced the strength of the final sintered parts. As mentioned above, the particle size also has a strong influence on the success of the method: the smaller the particles, the more binder is required to wet the particle surface. Very small particles could cause non-uniform spreading, resulting in deformation of the part, formation of cracks and delamination during the SLS fabrication of the first layers. Larger particles are easier to handle but could lead to poor mechanical properties. For particles of approx. 16 µm diameter good results were achieved. For the SLS process, an optimal energy density was found at 1 cal/cm^2. At lower energy density, delamination between layers occurred. Higher energy densities led to improved densification, but also to dimensional inaccuracies. While keeping the energy density constant at 1 cal/cm^2, the influence of scan speed and laser energy was analysed. It could be shown that the compressive strength of the scaffolds was increased with increasing laser energy (3 – 5 W) and, consequently, increasing scan speed (305 – 508 mm/s). Thus, even if the energy density is constant, higher laser energy is favourable, as owing to the higher laser energy the polymeric binder in the previously scanned regions is re-melted and re-distributed also into any residual voids, thus reducing the microporosity of the SLS green part. After SLS, conventional debinding and sintering steps have to be applied to remove the polymeric binder and to sinter the glass matrix. Dense and macroporous samples were fabricated and sintered at 700 °C below the crystallization temperature of 13 – 93 glass. The compressive strength of the fabricated macroporous scaffolds (~ 60 % porosity) was measured to be up to 41 MPa, while samples without additional macropores reached a compressive strength of up to 157 MPa. The same group showed that 13 – 93 glass scaffolds with macropores in the range of 300 – 800 µm could be fabricated [55].

Bioactivity and biocompatibility tests on SLS-processed 13 – 93 scaffolds have shown favourable results. Within one week of immersion in SBF, the formation of HA crystals was observed. However, the compressive strength of the scaffolds was reduced by 38 % after six weeks of immersion in SBF. *In vitro* tests with MLO-A5 line of mouse late-osteoblast, early osteocyte cells, for two and four days showed good attachment of the cells via lamellipodia and filopodia and favourable cell growth on the scaffolds [55].

Apatite/mullite composite scaffolds have also been fabricated using the indirect SLS process [56]. For this, a glass with the composition $4.5SiO_2 3Al_2O_3 1.6P_2O_5 3CaO_2 CaF_2$ (molar ratio) was melt-quenched and milled to a particle size of 45 – 90 µm. The glass frit was mixed with 5 % acrylic binder and fused by a CO_2-laser with a laser power of 100 W, a scan speed of 250 mm/s and a scan overlap of 50 % of the laser beam diameter of 1.1 mm. The layer thickness was 0.25 mm. After the SLS process, the samples were sintered and crystallised to apatite/mullite in a preheated oven at 1200 °C for 1 h. Although bioactivity by soaking in SBF revealed no formation of an apatite layer, *in vitro* experiments of the SLS apatite/mullite composite samples with MG-63 cells demonstrated good cell viability and no negative effects of the material on cell morphology. In addition, *in vivo* experiments, with SLS samples (bulk cylinders measuring 4 mm in diameter and 10 mm in length) implanted into the metaphysis of the tibiae of mature rabbits for four weeks, gave no signs of negative or inflammatory response. Progressive bone growth was observed up to the surface of and into the porous SLS samples.

In related studies, apatite/wollastonite composites were fabricated using the indirect SLS process [57]. Again, the glass frit of 45 – 90 µm particle size was mixed with 5 % acrylic binder and was then processed by means of laser sintering. Subsequently, sintering (including simultaneous crystallisation) was performed, with careful control of nucleation and growth using dwell times at specific temperatures. The indirect SLS method resulted in apatite/wollastonite samples with interconnecting porosity. Impregnation of these samples with a 50 % P_2O_5-40 % CaO-10 % Na_2O glass reduced porosity to only a few closed pores. In this way, the flexural strength could be increased from 35 to 100 MPa. In SBF experiments an apatite layer began to form after one day and covered the surface completely after seven days. During *in vitro* cultivation of human MSCs on the SLS scaffolds, a confluent cell monolayer was observed that remained for the whole duration of the 21 days of culture.

Altogether it can be stated that, although the dimensional accuracy seems to be better for the indirect SLS process, the direct SLS process is also an attractive technique for the fabrication of bioactive glass or silicate bioceramic scaffolds, as no additional post-processing step is required, which reduces the fabrication time and costs.

V. Dispense Plotting

Another fabrication method in AM technology to generate porous 3D implant geometries is dispense plotting [58, 59]. The name of this technique varies strongly and different synonyms can be found in the literature: direct ink writing, direct-write assembly, robocasting, (paste) extrusion free-forming, fused deposition modelling. In general, during processing a paste-like material is extruded through a nozzle onto a building platform. The major advantage of dispense plotting is that different materials like biopolymers, hydrogels, ceramics and composites can be used to manufacture scaffolds.

As mentioned above, challenges in constructing bone scaffolds involve the realization of three-dimensional interconnecting porosity to allow cell ingrowth and communication, a high total porosity (more than 60 %) and the optimization of pore sizes (250 – 500 µm) for bone healing and vascularisation. Besides these biological requirements, the used biomaterials should offer sufficient mechanical stability and controllable degradation behaviour.

In detail, in the dispense-plotting method, scaffolds are produced line-by-line and layer-by-layer out of rods. A paste-like slurry is filled into a cartridge and extruded by means of pressurized air through a fine nozzle while the

cartridge moves computer-controlled in x- and y-directions (Fig. 8). Essential for this method is the availability of a slurry with high solids loading and thixotropic flow behaviour. The slurry can be extruded through fine nozzles, but it remains a stable rod when deposited onto the building platform. By rotating the direction of the extruded rods by a certain angle from layer to layer, three-dimensional scaffolds are produced. By changing the lay-down-pattern, e.g. 0/90° or 0/60/120°, the pore geometry can be varied. The rod diameter can be controlled by the nozzle diameter and the deposition speed, while the pore size can be determined by the CAD data, which controls the plotter. In most cases, after fabrication and drying, the scaffolds are debinded and sintered to densify the structure.

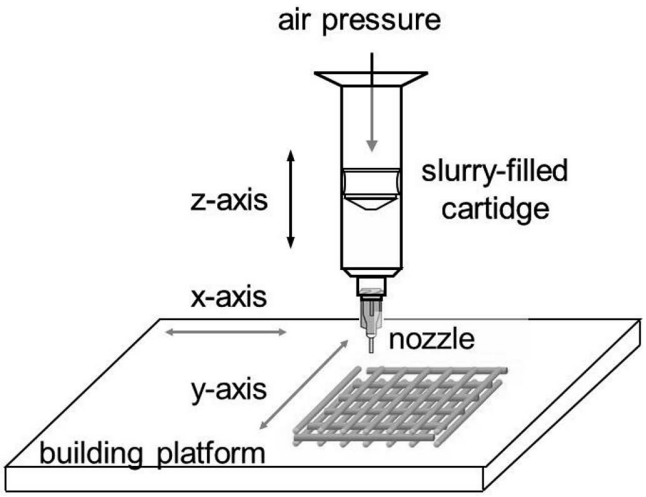

Fig. 8: Principle of dispense-plotting: paste-like slurry is extruded by means of air pressure through a fine nozzle and deposited as rods onto a building platform.

The challenge to obtain suitable scaffolds with the dispense plotting technique includes optimizing the following processing parameters:

- Thixotropic property of the slurry
- Air pressure
- Nozzle diameter
- Temperature
- Plot velocity
- Distance between nozzle and building platform
- Diameter and distance between the struts

Addressing these challenges, Eqtesadi *et al.* recently reported the fabrication of 45S5 Bioglass® scaffolds by dispense plotting and final sintering at 1000 °C [60]. In this study 45 vol% of 4.3 -µm-sized BG particles were added to deionized water and mixed with 1 wt% (relative to solid content) carboxymethyl cellulose. The slurry was plotted using a nozzle with diameter of 410 µm and a plot velocity of 10 mm/s. The sintered scaffolds showed porosity in the range of 60 – 80 % with a compressive strength of approx. 13 MPa. Compared to bone properties, this approach showed very promising results, although the *in vitro* or *in vivo* behaviour of the scaffolds has not been tested yet. Besides the 45S5 melt-derived bioactive glass composition, 13 – 93 (53 % SiO_2-6 % Na_2O-12 % K_2O-5 % MgO-20 % CaO-4 %P_2O_5, wt%) glass has been also used for preparing scaffolds with the dispense plotting technique [61]. In this study 13 – 93 glass particles (40 vol%) were mixed with a 20 wt% Pluronic® (F-127) solution, then scaffolds were manufactured and finally sintered at 700 °C. The resulting scaffolds exhibited a porosity of 47 % and a compressive strength of 86 ± 9 MPa (as-fabricated), where the relatively high value of the mechanical strength can be explained by the low porosity. Interestingly, Deliormanli *et al.* [62] studied dispense-plotted scaffolds composed of 13 – 93 and borate glasses. The scaffolds showed a porosity of 45 – 60 % depending on the macro pores. After four weeks subcutaneous implantation in rats, all dispense-plotted scaffolds were surrounded by fibrous tissue and blood vessel formation was observed in the macropores. Mesoporous bioactive ceramics and glasses (MBGs), which are derived from the sol-gel process, are being increasingly considered to fabricate bone tissue scaffolds [63]. In addition to their excellent bioactivity, MBGs can be loaded and functionalized with different bioactive molecules or drugs. In a study of Wu *et al.* [64], the manufacturing of scaffolds composed of 86 % MBG and 14 % PVA was demonstrated. After plotting, the scaffolds were dried at 40 °C overnight. The resulting scaffolds exhibited a porosity of 60 % with a compressive strength of 16 MPa. Additionally, *in vitro* tests showed good compatibility to bone marrow stromal cells. In related research, Zhang *et al.* [65] manufactured strontium-containing mesoporous bioactive glass (Sr-MBG) scaffolds by means of dispense plotting. The slurry used was prepared by mixing Sr-MBG particles (45 µm) and polyvinyl alcohol in a weight ratio of 50:50. The applied pressure ranged from 1.5 to 3.8 bar and the plot velocity was in the range 9 – 12 mm/s. Using a nozzle with a diameter of 400 µm, 15 layers were plotted. The estimated porosity was approx. 70 % and the compressive strength was 9 MPa. The *in vitro* properties of Sr-MBG scaffolds were evaluated by studying the forming ability of apatite and the proliferation as well as osteogenic differentiation of osteoblast-like cells MC3T3-E1. The results showed that Sr-MBG scaffolds exhibited suitable apatite-forming ability and enhanced cell activity. Combining MBGs with biopolymers like alginate is a further promising approach to generate bioactive scaffolds for bone tissue engineering with this technique [66]. The MBG-alginate paste showed superior processing ability for the plotting process. The scaffolds were shown to exhibit bioactive properties as well as enhanced attachment and alkaline phosphatase activity of human-bone-marrow-derived mesenchymal stem cells. Compared to dispense plotting, in fused deposition modelling a small temperature-controlled extruder is used to allow thermoplastic materials like PCL, PLA and PLGA to be deposited onto a platform layer-by-layer to form 3D structures. Adding this kind of thermoplastic materials gives numerous different possibilities to form composite scaffolds. For example, PCL melted at 110 °C and mixed with 10 wt% 45S5 BG particles was extruded to form highly porous scaffolds with a porosity of up to 85 % [67]. The Young's modulus of these scaffolds ranged from 42 to 59 MPa. Furthermore, *in vitro* analysis with MC3T3-E1 cells showed no toxic effect of the manufactured scaffolds. Moreover, Yang *et al.* [68] have published a study about the fabrication of 3-hydroxybutyrate-co-3-hydroxyhexanoate scaffolds

which were coated afterwards with MBG [68]. The scaffolds were produced by melting the polymer at temperatures up to 170 °C, subsequently followed by the plotting process with a velocity of 5 mm/s. The produced scaffolds were then immersed into a MBG solution several times for 10 min. The resulting porosity decreased with the coating steps whereas the compressive strength was approx. 15 MPa. After seven days of incubation, a significant increase in apatite formation on the scaffold surfaces was detected, combined with improved behaviour of MSC.

Altogether, it can be stated that dispense plotting is, regarding the selection of materials, the most versatile technique compared to the other AMTs. Beside different bioactive glasses, several combinations of composites and hybrid materials can be considered. The mechanical stability of the parts is in general very high and can be further improved with the addition of support structures around delicate (brittle) geometrical features. In addition, new versions of plotters are often equipped with more than one cartridge, so that different materials can be combined in one printing process.

VI. Inkjet Printing

Inkjet printing is an additional AMT frequently used to fabricate metal, polymer and ceramic parts [69]. In this method, small amounts of liquids with dispersed particles are printed layer-by-layer. Before the next layer is added, the slurry must turn from a viscous liquid to a solid structure by drying in order to bear the weight of the next layers. There are two types of ink delivery systems for droplet-based writing, continuous and drop-on-demand ink-jet printing. To the authors' knowledge there is no publication about inkjet printing of bioactive glasses so far. However, silica-based sol-gel-derived materials have been inkjet-printed for biosensor applications [70]. It is likely that this AM method will be conveniently used to print MBG in future research efforts.

VII. Conclusions

In this review, we have highlighted a series of available state-of-the-art technologies to additively process bioactive glasses (e.g. 45S5, 13 – 93) and silicate bioceramics as well as combinations thereof. The potential use of these technologies has been considered mainly from the point of view of the density and mechanical properties of the produced components or scaffolds and based on *in-vitro* and *in-vivo* results. Advantages and disadvantages, as well as general limitations regarding material processability, were discussed from the manufacturing perspective. Using the listed additive manufacturing technologies (Stereolithographic Ceramic Manufacturing (SLCM/LCM), 3D-Printing, indirect and direct Selective Laser Sintering/Melting (SLS/SLM), Dispense Plotting and Inkjet Plotting) it is possible to produce dense or porous bioactive glass and bioceramic parts with potential medical applications (e.g. as bone replacement materials and bone tissue scaffolds). As recent data in the literature suggest, load-bearing, bone-replacing applications could become a reality for a variety of 3D components made from bioactive glasses and glass ceramics by AMTs. Stereolithographic Ceramic Manufacturing (SLCM) or 3D-printing show the highest promise to fulfil these mechanical demands. While SLCM enables superior feature resolution, its challenging raw material requirements (particle size and distribution) limit today's commercial availability of advanced glass and glass-ceramic powder formulations. 3D printing on the other hand deals with more coarse-grained powders, also enabling suitable mechanical properties with a reasonable structural accuracy in the sub-millimetre range. Direct SLS processing of bioactive glasses and bioceramics results in porous structures with rather poor mechanical strength. Nevertheless, owing to its benefit of direct manufacturing, it could be an economically interesting alternative for bone replacement structures in non-load-bearing applications. However, with indirect SLS the production of strong scaffolds with macroporous structures becomes possible, again using thermal post-processing steps. Dispense plotting offers an interesting alternative to other AMTs. While its main disadvantages are given by the low feature resolution and its limitations in manufacturing highly complex and delicate structures, a huge benefit is provided by the ability to easily combine different biomaterials during the printing process. Combinations of different inorganic phases (glasses, ceramics) and mixtures containing organic phases (biopolymers, bioactive molecules or drugs) are also possible.

On the material side, new trends can be also observed. In addition to the standard 45S5 Bioglass®, attractive results have been obtained with other BG formulations such as 13 – 93, boron-containing BGs and mesoporous bioactive glasses, which have been shown to be suitable for processing with most of the introduced additive manufacturing technologies, opening up broad opportunities for expanding the applications of these materials in the biomedical field.

Acknowledgements

Authors RD and ARB acknowledge financial support from the Emerging Fields Initiative of the University of Erlangen-Nuremberg (Project TOPbiomat).

References

1 Bertrand, P., Bayle, F., Combe, C., Goeuriot, P., Smurov, I.: Ceramic components manufacturing by selective laser sintering, *Appl. Surf. Sci.*, **254**, [4], 989 – 992, (2007).

2 Exner, H., Horn, M., Streek, A. Ullmann, F., Hartwig, L., Regenfuss, P., Ebert, R.: Laser micro sintering: A new method to generate metal and ceramic parts of high resolution with sub-micrometer powder, *Virtual Phys. Prototyp.*, **3**, [1], 3 – 11, (2008).

3 Kollenberg, W.: *Technical Ceramics*, in German, 2nd edition. Vulkan, Essen, Germany, 2009.

4 Götschel, I., Gutbrod, B., Travitzky, N., Roosen, A., Greil, P.: Processing of preceramic paper and ceramic green tape derived multilayer structures, *Adv. Appl. Ceram.*, **112**, [6], 358 – 365, (2013).

5 Windsheimer, H., Travitzky, N., Hofenauer, A., Greil, P.: Laminated object manufacturing of preceramic-paper-derived SiSiC composites, *Adv. Mater.*, **19**, [24], 4515 – 4519, (2007).

6 Novakova-Marcincinova, L., Novak-Marcincin, J., Barna, J., Torok, J.: Special materials used in FDM rapid prototyping technology application; pp. 73 – 76 in *2012 IEEE 16th Int. Conf. Intell. Eng. Syst. INES*. 2012.

7 Felzmann, R., Gruber, S., Mitteramskogler, G., Tesavibul, P., Boccaccini, A.R., Liska, R.,Stampfl, J.: Lithography-based additive manufacturing of cellular ceramic structures, *Adv. Eng. Mater.*, **14**, [12], 1052 – 1058, (2012).

8 Shahzad, K., Deckers, J., Kruth, J.P., Vleugels, J.: Additive manufacturing of alumina parts by indirect selective laser sintering and post processing, *J. Mater. Process. Technol.*, **213**, [9], 1484 – 1494, (2013).

9 D'haese, J., Van De Velde, T., Komiyama, A., Hultin, M., De Bruyn, H.: Accuracy and complications using computer-designed stereolithographic surgical guides for oral rehabilitation by means of dental Implants: A review of the literature, *Clin. Implant Dent. R.*, **14**, [3], 321 – 335, (2012).

10 Ozan, O., Turkyilmaz, I., Ersoy, A.E., McGlumphy, E.A., Rosenstiel, S.F.: Clinical accuracy of 3 different types of computed tomography-derived stereolithographic surgical guides in implant placement, *J. Oral Maxillofac. Surg.*, **67**, [2], 394 – 401, (2009).

11 Fluegge, T.V., Nelson, K., Schmelzeisen, R., Metzger, M.C.: Three-dimensional plotting and printing of an implant drilling Guide: simplifying guided implant surgery, *J. Oral Maxillofac. Surg.*, **71**, [8], 1340 – 1346, (2013).

12 Bibb, R., Eggbeer, D., Evans, P., Bocca, A., Sugar, A.: Rapid manufacture of custom-fitting surgical guides, *Rapid Prototyping J.*, **15,** [5], 346 – 354, (2009).

13 Kasparova, M.,Grafova, L., Dvorak, P., Dostalova, T., Prochazka, A., Eliasova, H., Prusa, J., Kakawand, S.: Possibility of reconstruction of dental plaster cast from 3D digital study models, *Biomed. Eng. OnLine*, **12**, [1], 49, (2013).

14 Wohlers, T., Caffrey, T.: *Wohlers Report- Additive Manufacturing and 3D printing state of the industry*. 2013.

15 Hutmacher, D.W., Sittinger, M., Risbud, M.V.: Scaffold-based tissue engineering: rationale for computer-aided design and solid free-form fabrication systems, *Trends Biotechnol.*, **22**, [7]. 354 – 362, (2004).

16 Zein, I., Hutmacher, D.W., Tan, K.C., Teoh, S.H.: Fused deposition modeling of novel scaffold architectures for tissue engineering applications, *Biomaterials*, **23**, [4], 1169 – 1185, (2002).

17 Sobral, J.M., Caridade, S.G., Sousa, R.A., Mano, J.F., Reis, R.L.: Three-dimensional plotted scaffolds with controlled pore size gradients: effect of scaffold geometry on mechanical performance and cell seeding efficiency, *Acta Biomater.*, **7**, [3], 1009 – 1018, (2011).

18 Shao, X.X., Hutmacher, D.W., Ho, S.T., Goh, J.C.H., Lee, E.H.: Evaluation of a hybrid scaffold/cell construct in repair of high-load-bearing osteochondral defects in rabbits, *Biomaterials*, **27**, [7], 1071 – 1080, (2006).

19 Seitz, H., Rieder, W., Irsen, S., Leukers, B., Tille, C.: Three-dimensional printing of porous ceramic scaffolds for bone tissue engineering, *J. Biomed. Mater. Res.,* **74** [2], 782 – 788, (2005).

20 Habibovic, P., Gbureck, U., Doillon, C.J., Bassett, D.C., van Blitterswijk, C.A., Barralet, J.E.: Osteoconduction and osteoinduction of low-temperature 3D printed bioceramic implants, *Biomaterials*, **29**, [7], 944 – 953, (2008).

21 Bartolo, P.J. da Silva, de Lemos, A.C.S., Pereira, A.M.H., Mateus, A.J.D.S., Ramos, C., Santos, C.D., Oliveira, D., Pinto, E. *et al.*: *High Value Manufacturing: Advanced research in virtual and rapid prototyping: Proceedings of the 6th international conference on advanced research in virtual and rapid prototyping, Leiria, Portugal, 1 – 5 October, 2013*. CRC Press, 2013.

22 Kumar, S., Kruth, J.-P.: Composites by rapid prototyping technology, *Mater. Des.*, **31**, [2], 850 – 856, (2010).

23 Knitter, R., Bauer, W.: Ceramic microfabrication by rapid prototyping process chains, *Sadhana*, **28**, [1 – 2], 307 – 318, (2003).

24 Doreau, F., Chaput, C., Chartier, T.: Stereolithography for manufacturing ceramic parts, *Adv. Eng. Mater.*, **2**, [8], 493 – 496, (2000).

25 Gruber, S.: Lithography-based additive manufacturing of alumina parts; PhD Thesis, Vienna University of Technology, Vienna, Austria, 2013.

26 Felzmann, R., Gruber, S., Mitteramskogler, G., Pastrama, M., Boccaccini, A.R., Stampfl, J.: Lithography-based additive manufacturing of customized bioceramic parts for medical applications; in *Biomed. Eng.* ACTAPRESS, Innsbruck, Austria, 2013.

27 Tesavibul, P., Felzmann, R., Gruber, S., Liska, R., Thompson, I., Boccaccini, A.R., Stampfl, J.: Processing of 45S5 Bioglass® by lithography-based additive manufacturing, *Mater. Lett.*, **74**, 81 – 84, (2012).

28 Gerhardt, L.-C., Boccaccini, A.R.: Bioactive glass and glass-ceramic scaffolds for bone tissue engineering, *Materials*, **3**, [7], 3867 – 3910, (2010).

29 Rahaman, M.N., Day, D.E., Sonny Bal, B., Fu, Q., Jung, S.B., Bonewald, L.F., Tomsia, A.P.: Bioactive glass in tissue engineering, *Acta Biomater.*, **7**, [6], 2355 – 2373, (2011).

30 Wu, C., Ramaswamy, Y., Zreiqat, H.: Porous diopside ($CaMgSi_2O6$) scaffold: A promising bioactive material for bone tissue engineering, *Acta Biomater.*, **6**, [6], 2237 – 2245, (2010).

31 Vitale-Brovarone, C., Verné, E., Robiglio, L., Appendino, P., Bassi, F., Martinasso, G., Muzio, G., Canuto, R.: Development of glass-ceramic scaffolds for bone tissue engineering: characterisation, proliferation of human osteoblasts and nodule formation, *Acta Biomater.*, **3**, [2], 199 – 208, (2007).

32 Gorustovich, A.A., Roether, J.A., Boccaccini, A.R.: Effect of bioactive glasses on Angiogenesis: A review of in vitro and in vivo evidences, *Tissue Eng. Part B Rev.*, **16**, [2], 199 – 207, (2010).

33 Hoppe, A., Güldal, N.S., Boccaccini, A.R.: A review of the biological response to ionic dissolution products from bioactive glasses and glass-ceramics, *Biomaterials*, **32**, [11], 2757 – 2774, (2011).

34 Gmeiner, R., Mitteramskogler, G., Stampfl, J., Boccaccini, A.R.: Stereolithographic ceramic manufacturing of high strength bioactive glass, *Int. J. Appl. Ceram. Technol.*, **12**, 38-45, (2015).

35 Mitteramskogler, G., Gmeiner, R., Felzmann, R., Gruber, S., Hofstetter, C., Stampfl, J., Ebert, J., Wachter, W. *et al.*: Light curing strategies for lithography-based additive manufacturing of customized ceramics, *Addit. Manuf.*, **1 – 4**, 110 – 118, (2014).

36 Wu, C., Chang, J.: A review of bioactive silicate ceramics, *Biomed. Mater.*, **8**, [3], 032001, (2013).

37 Fu, Q., Rahaman, M.N., Bal, B.S., Kuroki, K., Brown, R.F.: In vivo evaluation of 13 – 93 bioactive glass scaffolds with trabecular and oriented microstructures in a subcutaneous rat implantation model, *J. Biomed. Mater. Res. A*, **95A**, [1], 235 – 244, (2010).

38 Durand, L.A.H., Góngora, A., López, J.M.P., Boccaccini, A.R., Zago, M.P., Baldi, A., Gorustovich, A.: In vitro endothelial cell response to ionic dissolution products from boron-doped bioactive glass in the SiO_2-CaO-P_2O_5-Na_2O system, *J. Mater. Chem. B*, **2**, [43], 7620 – 7630, (2014).

39 Gu, Y., Huang, W., Rahaman, M.N., Day, D.E.: Bone regeneration in rat calvarial defects implanted with fibrous scaffolds composed of a mixture of silicate and borate bioactive glasses, *Acta Biomater.*, **9**, [11], 9126 – 9136, (2013).

40 Detsch, R., Guillon, O., Wondraczek, L., Boccaccini, A.R.: Initial attachment of rMSC and MG-63 cells on patterned Bioglass® substrates, *Adv. Eng. Mater.*, **14**, [3], B38 – B44, (2012).

41 Marchelli, G., Prabhakar, R., Storti, D., Ganter, M.: The guide to glass 3D printing: developments, methods, diagnostics and results, *Rapid Prototyp. J.*, **17**, [3], 187 – 194, (2011).

42 Bretcanu, O., Chatzistavrou, X., Paraskevopoulos, K., Conradt, R., Thompson, I., Boccaccini, A.R.: Sintering and crys-

tallisation of 45S5 Bioglass® powder, *J. Eur. Ceram. Soc.*, **29**, [16], 3299 – 3306, (2009).

43 Winkel, A., Meszaros, R., Reinsch, S., Müller, R., Travitzky, N., Fey, T., Greil, P., Wondraczek, L.: Sintering of 3D-printed Glass/HAp composites, *J. Am. Ceram. Soc.*, **95**, [11], 3387 – 3393, (2012).

44 Suwanprateeb, J., Sanngam, R., Suvannapruk, W., Panyathanmaporn, T.: Mechanical and in vitro performance of apatite-wollastonite glass ceramic reinforced hydroxyapatite composite fabricated by 3D-printing, *J. Mater. Sci. Mater. M.*, **20**, [6], 1281 – 1289, (2009).

45 Bergmann, C., Lindner, M., Zhang, W., Koczur, K., Kirsten, A., Telle, R., Fischer, H.: 3D printing of bone substitute implants using calcium phosphate and bioactive glasses, *J. Eur. Ceram. Soc.*, **30**, [12], 2563 – 2567, (2010).

46 Zocca, A., Gomes, C.M., Bernardo, E., Müller, R., Günster, J., Colombo, P.: LAS glass-ceramic scaffolds by three-dimensional printing, *J. Eur. Ceram. Soc.*, **33**, [9], 1525 – 1533, (2013).

47 Meszaros, R., Zhao, R., Travitzky, N., Fey, T., Greil, P., Wondraczek, L.: Three-dimensional printing of a bioactive glass, *Glass Technol. -Part A*, **52**, [4], 111 – 116, (2011).

48 Liu, J., Hu, H., Li, P., Shuai, C., Peng, S.: Fabrication and characterization of porous 45S5 glass scaffolds via direct selective laser sintering, *Mater. Manuf. Process.*, **28**, [6], 610 – 615, (2013).

49 Chen, Q.Z., Thompson, I.D., Boccaccini, A.R.: 45S5 Bioglass®-derived glass-ceramic scaffolds for bone tissue engineering, *Biomaterials*, **27**, [11], 2414 – 2425, (2006).

50 Gao, C., Liu, T., Shuai, C., Peng, S.: Enhancement mechanisms of graphene in nano-58S bioactive glass scaffold: mechanical and biological performance, *Sci. Rep.*, **4**, (2014).

51 Lorrison, J.C., Dalgarno, K.W., Wood, D.J.: Processing of an apatite-mullite glass-ceramic and an hydroxyapatite/phosphate glass composite by selective laser sintering, *J. Mater. Sci. Mater. M.*, **16**, [8], 775 – 781, (2005).

52 Deisinger, U.: Selective laser melting of calcium phosphate glass/hydroxyapatite composites, in: Proceedings of the 11th ECERS conference in Krakow, pp. 424 – 426, (2009).

53 Kolan, K.C.R., Leu, M.C., Hilmas, G.E., Velez, M.: Selective laser sintering of 13 – 93 bioactive glass, in: Proceedings of 21st annual international solid freeform fabrication symposium - an additive manufacturing conference, pp. 504 – 512, (2010).

54 Kolan, K.C.R., Leu, M.C., Hilmas, G.E., Velez, M.: Effect of material, process parameters, and simulated body fluids on mechanical properties of 13 – 93 bioactive glass porous constructs made by selective laser sintering, *J. Mech. Behav. Biomed. Mater.*, **13**, 14 – 24, (2012).

55 Kolan, K.C.R., Leu, M.C., Hilmas, G.E., Brown, R.F., Velez, M.: Fabrication of 13 – 93 bioactive glass scaffolds for bone tissue engineering using indirect selective laser sintering, *Biofabrication*, **3**, [2], 025004, (2011).

56 Goodridge, R.D., Wood, D.J., Ohtsuki, C., Dalgarno, K.W.: Biological evaluation of an apatite-mullite glass-ceramic produced via selective laser sintering, *Acta Biomater.*, **3**, [2], 221 – 231, (2007).

57 Wood, D.J., Dyson, J., Xiao, K., Dalgarno, K.W., Genever, P.: Processing and characterization of apatite-wollastonite porous scaffolds for bone tissue engineering, *Key Eng. Mater.*, **361 – 363,** 923 – 926, (2008).

58 Deisinger, U., Hamisch, S., Schumacher, M., Uhl, F., Detsch, R., Ziegler, G.: Fabrication of tailored hydroxyapatite Scaffolds: comparison between a direct and an indirect rapid prototyping technique, *Key Eng. Mater.*, **361 – 363**, 915 – 918, (2008).

59 Detsch, R., Dieser, I., Deisinger, U., Uhl, F., Hamisch, S., Ziegler, G., Lipps, G.: Biofunctionalization of dispense-plotted hydroxyapatite scaffolds with peptides: quantification and cellular response, *J. Biomed. Mater. Res. A*, **92**, [2], 493 – 503, (2010).

60 Eqtesadi, S., Motealleh, A., Miranda, P., Pajares, A., Lemos, A., Ferreira, J.M.F.: Robocasting of 45S5 bioactive glass scaffolds for bone tissue engineering, *J. Eur. Ceram. Soc.*, **34**, [1], 107 – 118, (2014).

61 Liu, X., Rahaman, M.N., Hilmas, G.E., Bal, B.S.: Mechanical properties of bioactive glass (13 – 93) scaffolds fabricated by robotic deposition for structural bone repair, *Acta Biomater.*, **9**, [6], 7025 – 7034, (2013).

62 Deliormanli, A.M., Liu, X., Rahaman, M.N.: Evaluation of borate bioactive glass scaffolds with different pore sizes in a rat subcutaneous implantation model, *J. Biomater. Appl.*, **28**, [5], 643 – 653, (2014).

63 Houmard, M., Fu, Q., Saiz, E., Tomsia, A.P.: Sol-gel method to fabricate CaP scaffolds by robocasting for tissue engineering, *J. Mater. Sci. Mater. M.*, **23,** [4], 921 – 930, (2012).

64 Wu, C., Luo, Y., Cuniberti, G., Xiao, Y., Gelinsky, M.: Three-dimensional printing of hierarchical and tough mesoporous bioactive glass scaffolds with a controllable pore architecture, excellent mechanical strength and mineralization ability, *Acta Biomater.*, **7**, [6], 2644 – 2650, (2011).

65 Zhang, J., Zhao, S., Zhu, Y., Huang, Y., Zhu, M., Tao, C., Zhang, C.: Three-dimensional printing of strontium-containing mesoporous bioactive glass scaffolds for bone regeneration, *Acta Biomater.*, **10**, [5], 2269 – 2281, (2014).

66 Luo, Y., Wu, C., Lode, A., Gelinsky, M.: Hierarchical mesoporous bioactive glass/alginate composite scaffolds fabricated by three-dimensional plotting for bone tissue engineering, *Biofabrication*, **5**, [1], 015005, (2013).

67 Poh, P.S.P., Hutmacher, D.W., Stevens, M.M., Woodruff, M.A.: Fabrication and in vitro characterization of bioactive glass composite scaffolds for bone regeneration, *Biofabrication*, **5**, [4], 045005, (2013).

68 Yang, S., Wang, J., Tang, L., Ao, H., Tan, H., Tang, T., Liu, C.: Mesoporous bioactive glass doped-poly (3-hydroxybutyrate-co-3-hydroxyhexanoate) composite scaffolds with 3-dimensionally hierarchical pore networks for bone regeneration, *Colloid. Surface. B*, **116**, 72 – 80, (2014).

69 Calvert, P.: Inkjet printing for materials and devices, *Chem. Mater.*, **13**, [10], 3299 – 3305, (2001).

70 Monton, M.R.N., Forsberg, E.M., Brennan, J.D.: Tailoring Sol-Gel-derived silica materials for optical biosensing, *Chem. Mater.*, **24**, [5], 796 – 811, (2011).